Article

Aryl Vinyl Sulfonates and Sulfones as Active Site-Directed and Mechanism-Based Probes for Protein Tyrosine Phosphatases

Sijiu Liu, Bo Zhou, Heyi Yang, Yantao He, Zhong-Xing Jiang, Sanjai Kumar, Li Wu, and Zhong-Yin Zhang

J. Am. Chem. Soc., **2008**, 130 (26), 8251-8260 • DOI: 10.1021/ja711125p • Publication Date (Web): 04 June 2008

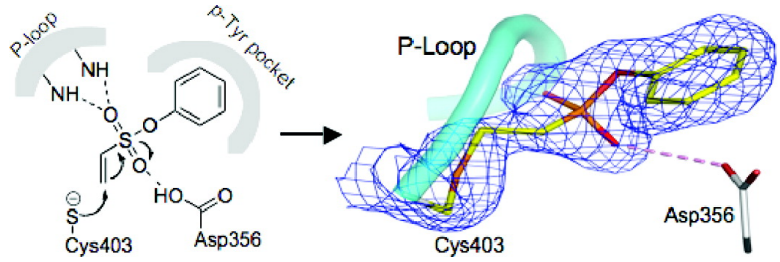

More About This Article

Additional resources and features associated with this article are available within the HTML version:

- Supporting Information
- Access to high resolution figures
- Links to articles and content related to this article
- Copyright permission to reproduce figures and/or text from this article

View the Full Text HTML

J|A|C|S
ARTICLES

Published on Web 06/04/2008

Aryl Vinyl Sulfonates and Sulfones as Active Site-Directed and Mechanism-Based Probes for Protein Tyrosine Phosphatases

Sijiu Liu, Bo Zhou, Heyi Yang,† Yantao He, Zhong-Xing Jiang, Sanjai Kumar,‡ Li Wu, and Zhong-Yin Zhang*

Department of Biochemistry and Molecular Biology, Indiana University School of Medicine, 635 Barnhill Drive, Indianapolis, Indiana 46202

Received December 14, 2007; E-mail: zyzhang@iupui.edu

Abstract: Protein tyrosine phosphatases (PTPs) play key roles in the regulation of normal and pathological processes ranging from cell proliferation, differentiation, metabolism, and survival to many human diseases including cancer and diabetes. Functional studies of PTP can be greatly facilitated by small molecule probes that covalently label the active site of a PTP through an activity-dependent chemical reaction. In this article, we characterize phenyl vinyl sulfonate (PVSN) and phenyl vinyl sulfone (PVS) as a new class of mechanism-based PTP probes. PVSN and PVS inactivate a broad range of PTPs in a time- and concentration-dependent fashion. The PVSN- and PVS-mediated PTP inactivation is active site-directed and irreversible, resulting from a Michael addition of the active-site Cys Sγ onto the terminal carbon of the vinyl group. Structural and mechanistic analyses reveal the molecular basis for the preference of PVSN/PVS toward the PTPs, which lies in the ability of PVSN and PVS to engage the conserved structural and catalytic machinery of the PTP active site. In contrast to early α-bromobenzyl phosphonate-based probes, PVSN and PVS are resistant to solvolysis and are cell-permeable and thus hold promise for in vivo applications. Collectively, these properties bode well for the development of aryl vinyl sulfonate/sulfone-based PTP probes to interrogate PTP activity in complex proteomes.

Introduction

Protein phosphorylation, targeted to tyrosine residues, plays a central role in regulating a diverse range of fundamental cellular processes, including growth, differentiation, metabolism, cell cycle progression, cell adhesion and migration, ion channel activity, immune response, and apoptosis/survival.[1] In vivo, tyrosine phosphorylation is reversible and dynamic and is governed by the opposing activities of protein tyrosine kinases and protein tyrosine phosphatases (PTPs). Although the importance of protein tyrosine kinases in cell physiology has long been established, the PTPs have garnered increasing recognition as critical modulators of signaling events regulated by tyrosine phosphorylation.[2] The PTPs constitute a large family of enzymes,[3] and dysfunction in PTPs has been linked to the etiology of several human diseases, including cancer, diabetes and obesity, and autoimmune disorders.[4] For example, PTP1B is implicated as a negative regulator of insulin and leptin-mediated processes, and mice lacking functional PTP1B exhibit increased sensitivity toward insulin and are resistant to obesity.[5,6] In addition, PTPs can also potentiate, rather than antagonize, actions of protein tyrosine kinases. Thus, SHP2 is a positive mediator of growth factor signaling, and gain-of-function mutations in SHP2 are associated with Noonan syndrome and several forms of leukemia.[7,8]

Our current knowledge of the PTPs has been mostly derived from experiments using gene knockout or overexpression techniques. As discussed above, plausible biological functions have been documented for a number of PTPs, and it is clear that phosphate removal by the PTPs can either enhance or antagonize a cellular process. Unfortunately, genetic approaches do not provide an adequate view of the temporal, spatial, and dynamic properties of the PTPs in cell signaling. Given the large number and complexity of PTPs in cell physiology, new strategies are needed for integrated analysis of the PTPs in the

† Current address: Mount Sinai School of Medicine, 1425 Madison Avenue, New York, NY 10029.

‡ Current address: Queens College, 65-30 Kissena Blvd., Flushing, NY 11367.

(1) Hunter, T. *Philos. Trans. R. Soc. London, Ser. B* **1998**, *353*, 583–605.
(2) Tonks, N. K. *Nat. Rev. Mol. Cell Biol.* **2006**, *7*, 833–846.
(3) Alonso, A.; Sasin, J.; Bottini, N.; Friedberg, I.; Friedberg, I.; Osterman, A.; Godzik, A.; Hunter, T.; Dixon, J.; Mustelin, T. *Cell* **2004**, *117*, 699–711.
(4) Zhang, Z.-Y. *Curr. Opin. Chem. Biol.* **2001**, *5*, 416–423.
(5) Elchelby, M.; Payette, P.; Michaliszyn, E.; Cromlish, W.; Collins, S.; Lee Loy, A.; Normandin, D.; Cheng, A.; Himms-Hagen, J.; Chan, C.-C.; Ramachandran, C.; Gresser, M. J.; Tremblay, M. L.; Kennedy, B. P. *Science* **1999**, *283*, 1544–1548.
(6) Klaman, L. D.; Boss, O.; Peroni, O. D.; Kim, J. K.; Martino, J. L.; Zabolotny, J. M.; Moghal, N.; Lubkin, M.; Kim, Y. B.; Sharpe, A. H.; Stricker-Krongrad, A.; Shulman, G. I.; Neel, B. G.; Kahn, B. B. *Mol. Cell. Biol.* **2000**, *20*, 5479–5489.
(7) Tartaglia, M.; Mehler, E. L.; Goldberg, R.; Zampino, G.; Brunner, H. G.; Kremer, H.; van der Burgt, I.; Crosby, A. H.; Ion, A.; Jeffery, S.; Kalidas, K.; Patton, M. A.; Kucherlapati, R. S.; Gelb, B. D. *Nat. Genet.* **2001**, *29*, 465–468.
(8) Tartaglia, M.; Niemeyer, C. M.; Fragale, A.; Song, X.; Buechner, J.; Jung, A.; Hahlen, K.; Hasle, H.; Licht, J. D.; Gelb, B. D. *Nat. Genet.* **2003**, *34*, 148–150.

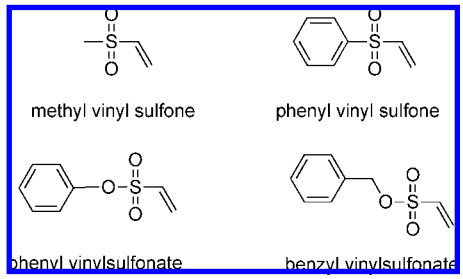

Figure 1. Structures of methyl vinyl sulfone, phenyl vinyl sulfone, phenyl vinyl sulfonate, and benzyl vinyl sulfonate.

whole proteome. To interrogate the functional complexity of the proteomes, powerful chemical reagents have been developed for targeted analysis of individual protein families.[9] In particular, mechanism-based probes are available for covalent labeling of the cysteine and serine hydrolases, providing new insights into our understanding of these two families of proteases in cell biology and in diseases.[10,11] In addition to profiling the functional state of enzymes, mechanism-based probes are also seeing application in drug discovery, target identification, and discovery of previously uncharacterized enzyme activity.[9]

To develop class-selective PTP probes, 4-fluromethylaryl phosphate was initially examined[12] as its hydrolysis generates a highly reactive quinone methide intermediate, which alkylate nucleophiles at, or near, the phosphatase active site.[13] Unfortunately, 4-fluromethylaryl phosphate is not specific for the PTPs, as the diffusible, unmasked quinone methide electrophile will nonspecifically label any nearby proteins. Consequently, chemical probes based on 4-fluromethylaryl phosphate lack the specificity required for profiling PTP activity. More recently, we reported several α-bromobenzyl phosphonate-based probes with extremely high selectivity for the PTPs.[14,15] When attached to appropriate affinity or fluorescent tags, these probes enable the identification and visualization of the labeled PTPs in complex proteomes. One major drawback for α-bromobenzyl phosphonate is the exceedingly low membrane permeability, which limits its usefulness as a research tool to globally characterize PTP activity in live cells.

The current dearth of cell-permeable covalent probes for PTPs stands as a significant challenge for investigators interested in mechanism-based profiling of this large enzyme class. As a first step toward the development of small molecule modulators of PTP activity inside the cell, we describe the characterization of aryl vinyl sulfonates and sulfones (Figure 1) as cell-permeable, mechanism-based probes for the PTPs. We show that the aryl vinyl sulfonates and sulfones inactivate a broad range of PTPs in a time- and concentration-dependent fashion. We establish that PTP inactivation by these compounds is active site-directed and irreversible. We provide evidence that these probes form a covalent adduct with PTPs, involving the active site Cys residue. These properties bode well for the application of the aryl vinyl sulfonate- and sulfone-based probes for functional characterization of the PTPs, thereby enhancing our understanding of the roles of PTPs in both health and diseases.

Materials and Methods

Materials. Methyl vinyl sulfone (MVS), phenyl vinyl sulfone (PVS), and phenyl vinyl sulfonate (PVSN) were obtained from Aldrich. PEG and buffers for crystallization were purchased from Hampton Research Co. *p*-Nitrophenyl phosphate (*p*NPP) was purchased from Fluke Co. Antiphosphotyrosine (pY20) polyclonal antibody was from B. D. Biosciences. Dithiothreitol (DTT), iodoacetamide, urea, ammonium bicarbonate, and acetonitrile were provided by Fisher. Formic acid was purchased from E. Merck. α-Cyano-4-hydroxycinnamic acid and modified sequencing grade trypsin were purchased from Sigma. $Ziptip_{c18}$ was obtained from Millipore. Dulbecco's modified Eagle's medium (DMEM) and fetal bovine serum were purchased from ATCC. Penicillin and streptomycin were purchased from Cellgrow. EDTA-free complete protease inhibitor cocktail tablets were purchased from Roche. All other chemicals and reagents were of the highest grade commercially available.

Synthesis of Benzyl Vinyl Sulfonate. 2-Chloro-1-ethane-sulfonylchloride (0.2 mL, 1.91 mmol) dissolved in anhydrous dichloromethane (5 mL) and benzyl alcohol (0.2 mL, 1.93 mmol) was treated, at 0 °C, with triethylamine (0.54 mL, 3.87 mmol). After 0.5 h, the reaction mixture was concentrated and the crude residue was purified by flash chromatography on silica gel (6% ethyl acetate in hexanes) to provide benzyl vinyl sulfonate (313 mg, 83% yield) as colorless oil. ^{1}H NMR (300 MHz, $CDCl_3$) δ 7.382 (m, 5H), 6.516−6.362 (m, 2H), 6.066 (d, J = 8.7 Hz, 1H), 5.149 (s, 2H); LC−ESI MS (*m*/*z*): 199 (M + 1).

Synthesis of Alkyne-Labeled Biotin. [16] *N*-(3-Dimethylaminopropyl)-*N*′-ethylcarbodiimide hydrochloride (920 mg, 4.8 mmol) was added to a solution of biotin (1 g, 4.1 mmol) and *N*-hydroxysuccinimide (510 mg, 4.4 mmol) in DMF (50 mL). The reaction solution was concentrated after 24 h at room temperature. The residue was washed by methanol three times, and the solvent was removed to yield a white solid, which was directly dissolved in DMF (100 mL). To this solution was added 0.48 mL of propargylamine (7.0 mmol) and 1.4 mL of triethylamine (10 mmol), and the solution was stirred at room temperature for 24 h. Subsequently, the reaction solution was concentrated in vacuum. Chromatography of the residue (MeOH/$CHCl_3$, 10/1) gave the alkyne-labeled biotin (682 mg, yield 61%). ^{1}H (CD_3OD, 500 MHz) δ 1.76 (quintet, J = 7.55 Hz, 2H), 1.90−2.10 (m, 4H), 2.53 (t, J = 7.3 Hz, 2H), 2.89 (t, J = 2.5 Hz, 1H), 2.93−3.03 (m, 4H), 3.24 (dd, J = 12.7 Hz, 5 Hz, 1H), 3.52 (m, 1H), 4.26 (d, J = 2.6 Hz, 2H), 4.62 (dd, J = 7.8 Hz, 4.5 Hz, 1H), 4.80 (dd, J = 7.9 Hz, 4.9 Hz, 1H); LC−MS (ESI) *m*/*z*: 282.1 $[M + 1]^+$.

Synthesis of Azide-Tagged PVSN Probe. To a stirred solution of 4-(bromomethyl)phenol (18.7 g, 100 mmol) in DMF (200 mL) was added sodium azide (7.8 g, 120 mmol), and the resulting solution was stirred for 4 h at room temperature. Then, the reaction mixture was diluted with EtOAc (600 mL) and washed with brine (100 mL, three times). The organic layer was dried with Na_2SO_4, filtrated through a pad of silica gel, and concentrated to give crude 4-(azidomethyl)phenol as a clear oil (11.3 g, yield 76%), which was used without further purification. 2-Chloroethanesulfonylchloride (15.0 g, 92 mmol) was added to a stirred solution of 4-(azidomethyl)phenol (11.3 g, 76 mmol) in CH_2Cl_2 (400 mL) at 0 °C. Then, ice-cold trimethylamine (39.9 mL, 276 mmol) was added in one portion at 0 °C. After 0.5 h, the reaction mixture was washed with cold 10% aqueous Na_2CO_3 (100 mL, three times), 2N HCl (100 mL), and water (100 mL), and the organic layer was dried with Na_2SO_4 and concentrated to give a residue that was purified by flash chromatography on silica gel (CH_2Cl_2/hexane =

(9) Evans, M. J.; Cravatt, B. F. *Chem. Rev.* **2006**, *106*, 3279–3301.
(10) Liu, Y.; Patricelli, M. P.; Cravatt, B. F. *Proc. Natl. Acad. Sci. U.S.A.* **1999**, *96*, 14694–14699.
(11) Greenbaum, D.; Medzihradszky, K. F.; Burlingame, A.; Bogyo, M. *Chem. Biol.* **2000**, *7*, 569–581.
(12) Lo, L.-C.; Pang, T.-L.; Kuo, C.-H.; Chiang, Y.-L.; Wang, H.-Y.; Lin, J.-J. *J. Proteome Res.* **2002**, *1*, 35–40.
(13) Myers, J. K.; Widlanski, T. S. *Science* **1993**, *262*, 1451–1453.
(14) Kumar, S.; Zhou, B.; Liang, F.; Wang, W.-Q.; Huang, Z.; Zhang, Z.-Y. *Proc. Natl. Acad. Sci. U.S.A.* **2004**, *101*, 7943–7948.
(15) Kumar, S.; Zhou, B.; Liang, F.; Yang, H.; Wang, W.-Q.; Zhang, Z.-Y. *J. Proteome Res.* **2006**, *5*, 1898–1905.
(16) Lin, P.-J.; Ueng, S.-H.; Yu, S.-C.; Jan, M.-D.; Adak, A. K.; Yu, C.-C.; Lin, C.-C. *Org. Lett.* **2007**, *9*, 2131–2134.

1/3) to give 4-(azidomethyl)phenyl ethenesulfonate (azide-tagged PVSN probe) (14.75 g, yield 67%). ^{1}H NMR (500 MHz, $CDCl_3$) δ 7.36 (m, 2H), 7.26 (m, 2H), 6.68 (dd, J = 16.7 Hz, 9.9 Hz, 1H), 6.38 (d, J = 16.7 Hz, 1H), 6.19 (d, J = 9.9 Hz, 1H), 4.38 (s, 2H); ^{13}C NMR (125.9 MHz, $CDCl_3$) δ 149.2, 134.8, 132.1, 131.8, 129.5, 122.6, 53.9; MS (ESI) m/z: 212 ($(M + 1 - N_2)^+$), 197 ($(M + 1 - N_3)^+$).

PTPs and Non-PTP Proteins. The catalytic domain (residues 163−468) of YopH was expressed in *Escherichia coli* and purified as described.[17] Other recombinant PTPs were expressed and purified as described previously.[18–20] Non-PTP enzymes were purchased from Sigma-Aldrich and stored at −20 °C.

Kinetic Characterization of PTP Inactivation by Vinyl Sulfonates and Sulfones. PTP inactivation by the vinyl sulfonates and sulfones was studied at 25 °C in a pH 6 buffer containing 50 mM sodium succinate, 1 mM EDTA, and ionic strength of 150 mM adjusted with NaCl. At appropriate time intervals, aliquots of 2 μL were removed from the reaction and added into a 200-μL solution containing 20 mM *p*NPP in pH 6.0 buffer at 30 °C.[14] The kinetic parameters of the inactivation reaction were obtained by fitting the data to the following equations:

$$\frac{A_t}{A_0} = \frac{A_\infty}{A_0} - \left(\frac{A_0 - A_\infty}{A_0}\right)\exp(-k_{obs} \cdot t) \quad (1)$$

$$k_{obs} = \frac{k_i \times [I]}{K_I + [I]} \quad (2)$$

LC−MS Analysis. An electrospray ion trap mass spectrometer (LCQ DECA XP plus, Thermo Finnigan) coupled with an online HPLC (LC10 AD VP, Shimadzu) was used for measurement of the molecular weight of proteins. A 1.0 × 25 mm C8 column (5-μm particle diameter, 300 Å pore size, VYDAC) with mobile phases A (0.1% formic acid in water) and B (0.1% formic acid in acetonitrile) was used to desalt and separate proteins by a linear gradient 5−45% of mobile phase B over 30 min at a flow rate of 25 μL/min. Desalted proteins were eluted directly to mass spectrometer for molecular weight measurement. Molecular weights of proteins were calculated by deconvolution of the multicharged ions formed by electrospray ionization (ESI) using Bioworks software (Thermo Finnigan).

Protein Digestion and MALDI-TOF Analysis. YopH proteins were incubated at 56 °C for 30 min in a solution containing 10 mM DTT and 8 M urea. Subsequently, 50 mM iodoacetamide was introduced to alkylate the denatured and reduced proteins. The protein was digested with trypsin (protein/enzyme, 50/1) at 37 °C overnight. The resulting peptides were desalted using Ziptip$_{c18}$ before MALDI-TOF experiments. A volume of 0.5 μL of the desalted peptides was mixed with 0.5 μL of saturated α-cyano-4-hydroxycinnamic acid solution in 50% aqueous acetonitrile containing 0.1% trifluoroacetic acid and spotted on a MALDI-TOF target plate. The sample matrix solution was allowed to air dry at room temperature. Voyager DE STR MALDI-TOF (Applied Biosystems) was used to obtain mass spectra in positive and reflector mode.

LC−MS/MS Analysis. A 180-μm id × 15 cm column packed with 3-μm 100 Å C18 stationary phase was used for chromatography separation in an Ultimate HPLC system (Dionex). The pump flow rate was split 1:125 for a column flow rate of 1 μL/min. The column effluent was directly electrosprayed using the orthogonal metal needle source without further splitting. Mobile phase A was 0.1% formic acid in water, and phase B was 0.1% formic acid in acetonitrile. The separation of peptides was achieved with a gradient of 15−45% B in 30 min. A LCQ Deca XP ion-trap mass spectrometer (Thermo Finnigan) was used to analyze peptides eluted from the column. The instrument acquired one full-scan mass spectrum (300−2000 m/z) followed by three data-dependent MS/MS spectra at 36% normalized collision energy. Dynamic exclusion was configured to minimize the number of replicate MS/MS spectra by excluding the m/z of the previous 25 precursors selected for collision-induced dissociation.

Table 1. Crystallographic Data and Refinement Statistics

	YopH·PVS	YopH·PVSN
Crystal Parameters		
space group	$P2_12_12_1$	$P2_12_12_1$
Cell Dimensions (Å)		
a	46.8	49.2
b	54.0	55.6
c	96.9	97.5
Data Collection		
resolution (Å)	50−2.0	50−2.0
no. of unique reflections	17150	16289
completeness (%)	94.6	90.3%
redundancy	3.2	3.5
R_{merge}[a]	0.097	0.047
Refinement		
resolution limit (Å)	50−2.0	50−2.2
no. of reflections used ($F \geq 2\delta$ (F))	14611	12279
no. of protein atoms	2166	2166
no. of inhibitors	1	1
no. of waters	164	94
R_{work}[b]/R_{free}[c]	20.5/25.3	18.0/22.6
rms Deviations from Ideal Geometry		
bond length (Å)	0.0053	0.0060
bond angle (deg)	1.28	1.24
average B-factors (Å^2)	27.2	23.6

[a] $R_{merge} = \Sigma_h\Sigma_i|I(h)_i - \langle I(h)\rangle|/\Sigma_h\Sigma_i I(h)_i$ [b] $R_{work} = \Sigma_h|F(h)_{calcd} - F(h)_{obsd}|/\Sigma_h F(h)_{obsd}$, where $F(h)_{calcd}$ and $F(h)_{obsd}$ were the refined calculated and observed structure factors, respectively. [c] R_{free} was calculated for a randomly selected 3.3% (YopH·PVS) and 2.6% (YopH·PVSN) of the reflections that were omitted from refinement.

Preparation and Crystallization of the YopH·PVSN and YopH·PVS Complexes. YopH (10 mL, 1 mg/mL in 20 mM Bis-Tris, pH 6.0 buffer) was mixed with 30 μL of PVSN or PVS stock solution (100 mM, dissolved in DMSO) at 4 °C for covalent labeling. Mass spectrometry was used to track covalent adduct formation. After 7 days of reaction with PVSN or PVS at 4 °C, YopH was found to be completely modified by the compounds. The YopH solution was then concentrated at ∼7 mg/mL, frozen by liquid nitrogen, and stored at −80 °C for crystallization. Crystals of YopH·PVSN (coordinates deposited in the Protein Data Bank, accession number 3BLT) and YopH·PVS (PDB accession number 3BLU) were obtained at 18 °C by vapor diffusion in hanging drops. The conditions for getting YopH·PVSN and YopH·PVS crystals were similar. The protein drops were equilibrated against a reservoir solution containing 25% w/v poly(ethylene glycol) 3350, 100 mM NaCl, and 100 mM HEPES buffer (pH 7.0−8.0). The drops consisted of protein at a concentration of 7 mg/mL, diluted by an equal volume of the reservoir solution. The crystals of YopH·PVSN and YopH·PVS belong to space group $P2_12_12_1$ (Table 1).

X-ray Data Collection and Structural Determination. For X-ray data collection, the crystals were flash-cooled by liquid nitrogen in their original PEG solutions used for crystallization. X-ray data of YopH·PVSN were collected at 100 K on a Rigaku RU-300 rotating anode generator (Rigaku/MSC) equipped with focusing mirrors (MSC/Yale) and an R-AXIS IV++ image plate detector; X-ray data of YopH·PVS were collected at 100 K on the F2 station beamline of MacCHESS. The data were processed using the program HKL.[21] Statistics of the data processing are provided in Table 1.

(17) Zhang, Z.-Y.; Clemens, J. C.; Schubert, H. L.; Stuckey, J. A.; Fischer, M. W. F.; Hume, D. M.; Saper, M. A.; Dixon, J. E. *J. Biol. Chem.* **1992**, *267*, 23759–23766.
(18) Shen, K.; Keng, Y.-F.; Wu, L.; Guo, X.-L.; Lawrence, D. S.; Zhang, Z.-Y. *J. Biol. Chem.* **2001**, *276*, 47311–47319.
(19) Zhou, B.; Zhang, Z.-Y. *J. Biol. Chem.* **2002**, *277*, 13889–13899.
(20) Sun, J.-P.; Wu, L.; Fedorov, A. A.; Almo, S. C.; Zhang, Z.-Y. *J. Biol. Chem.* **2003**, *278*, 33392–33399.

To determine the structure of YopH·PVSN, YopH·*p*-nitrocatechol sulfate (*p*NCS) (PDB entry code 1PA9),[20] omitting the *p*NCS and solvent molecules, was used as a search model to calculate a difference Fourier map for YopH·PVSN with the coefficients $2F_o - F_c$ and calculated phases (where F_o and F_c are the observed and calculated structure factors, respectively). The structures were refined to 2.2 Å resolution with the program CNS,[22] first using simulated annealing at 3000 K, and then alternating positional and individual temperature factor refinement cycles. The progress of the refinement was evaluated by the improvement in the quality of the electron density maps and the reduced values of the conventional *R* factor ($R = \Sigma_h||F_o| - |F_c||/\Sigma_h|F_o|$) and the free *R* factor (2.6% of the reflections omitted from the refinement).[23] The electron density maps were inspected, and the model was modified on an interactive graphics workstation with the program O.[24] Finally, water molecules were added gradually as the refinement progressed. They were assigned in the $|F_o| - |F_c|$ difference Fourier maps with a 3δ cutoff level for inclusion in the model. The structure of YopH·PVS was solved using the structure of YopH·PVSN without the solvent molecules and PVSN as the search model. The structure was refined to 2.0 Å resolution with the program CNS.[22] The refinement statistics are shown in Table 1.

Effect of PVSN and PVS on Cellular Phosphotyrosine Level. COS-7 cells were grown in DMEM supplemented with 10% fetal bovine serum, penicillin (50 units/mL), and streptomycin (50 μg/mL) under a humidified atmosphere containing 5% CO_2. Nearly 80% confluent COS-7 cells were treated for 1 h with 0.5 and 1 mM PVSN, PVS, MVS, α-bromobenzyl phosphonate (BBP), or 1 mM sodium vanadate. Cells were washed twice using ice-cold PBS and lysed in a buffer containing 50 mM Tris-HCl (pH 7.5), 1% Triton X-100, 0.1% sodium deoxycholate, 150 mM NaCl, 1 mM Na_3VO_4, 15 mM NaF, and an EDTA-free complete protease inhibitor cocktail. Cell lysates were precleared by centrifugation at 15000 rpm for 15 min. Protein concentration was determined by the Bradford method. Protein samples (50 μg) were resolved by 10% SDS-PAGE and subjected to immunoblotting with antiphosphotyrosine antibody 4G10.

PTP Labeling with the PVSN Probe by Click Chemistry. Specific labeling of the desired PTP in a complex proteome with the azide-tagged PVSN probe and click chemistry was carried out using a procedure similar to that described previously.[25] Cell lysates from *E. coli* transformed with or without His_6-HePTP (50 μg of total protein) were incubated with 20 μM azide-tagged PVSN probe for 30 min at room temperature in a pH 6.0 buffer (50 mM sodium succinate, 1 mM EDTA, adjusted to the ionic strength of 150 mM with NaCl). Each protein sample (85 μL) was then treated with 0.125 mM alkyne-labeled biotin (2.5 μL, 5 mM stock in DMSO), followed by 1.25 mM tris(2-carboxyethyl)phosphine (TCEP) (2.5 μL, 50 mM stock in water), 0.127 mM tris(benzyltriazolylmethyl)amine (TBTA) (7.5 μL, 1.7 mM in DMSO), and 1.25 mM $CuSO_4$ (2.5 μL, 50 mM stock in water). The click reaction was allowed to proceed at room temperature on a shaker for 1 h. The reaction was then quenched by the addition of one volume of 2 × SDS loading buffer and heated at 90 °C for 5 min. Each sample was divided into halves, which were separated on a 12% SDS-PAGE (10 μg of total protein per lane). The samples from one gel were transferred to a nitrocellulose membrane and subjected to Western blot analysis using anti-Biotin antibody and anti-His_6 antibody. The second gel was Coomassie blue stained for protein visualization.

Results and Discussion

Unlike protein kinases, where tyrosine-specific and serine/threonine-specific kinases share sequence identity, the PTPs show no structural similarity with serine/threonine phosphatases or the broad specificity acid or alkaline phosphatases. The hallmark that defines the PTP superfamily is the active-site sequence (H/V)**C**(X)$_5$**R**(S/T), also called the PTP signature motif, in the catalytic domain. The PTPs share a conserved active site that recognizes phosphotyrosine (pTyr) and a common catalytic mechanism that utilizes a highly reactive nucleophilic Cys residue.[26] This Cys (Cys403 in the *Yersinia* PTP YopH) displays an unusually low pK_a of ~5[27] and is situated at the bottom of the pTyr-binding pocket (i.e., the active site) such that its Sγ atom is poised 3 Å from the phosphorus atom of pTyr.[28] In the catalytic mechanism, the active-site Cys initiates a nucleophilic attack on the phosphorus atom, leading to the formation of a thiophosphoryl enzyme intermediate. This step is assisted by a general acid (Asp356 in YopH), which is in close proximity to the scissile phenolic oxygen of pTyr. The active-site arginine (Arg409 in YopH) participates in binding of the pTyr substrate and stabilizes the transition state during catalysis. Hydrolysis of this covalent enzyme intermediate then completes the catalytic cycle.[26]

The involvement of Cys for nucleophilic catalysis has important implications for the development of mechanism-based PTP probes, where design strategies may exploit the extraordinary reactivity of the active-site thiol group. In this regard, we note that a number of vinyl sulfone derivatives act as irreversible inhibitors of the cysteine proteases.[29–31] Given the intrinsic affinity of the PTP active-site pocket for pTyr, we reasoned that aryl vinyl sulfones or sulfonates may serve as pTyr surrogates and function as mechanism-based PTP inactivators. In the following, we describe a structural and mechanistic study of PVSN and PVS as mechanism-based, cell-permeable PTP probes.

PVSN and PVS Are Active Site-Directed and Irreversible PTP Inactivators. To determine whether PVSN and PVS can function as mechanism-based PTP probes, we first examined their effect on PTP activity using *p*NPP as a substrate. Both compounds inactivated the *Yersinia* PTP, YopH, in a time- and concentration-dependent first-order process (Figure 2A). Similar results were obtained with several PTPs, including PTP1B, HePTP, DEP-1, VHR, PRL1, and the low molecular weight PTP (data not shown). Inactivation of the PTPs by PVSN and PVS appeared irreversible as extensive dialysis and/or buffer exchange of the reaction mixture failed to recover enzyme activity. Analysis of the pseudo-first-order rate constant as a function of inhibitor concentration showed that PVSN-mediated YopH inactivation displayed saturation kinetics (Figure 2B), yielding values for the equilibrium binding constant K_I and the

(21) Otwinowski, Z.; Minow, W. *Methods Enzymol.* **1997**, *176*, 307–326.
(22) Brünger, A. T.; Adams, P. D.; Clore, G. M.; DeLano, W. L.; Gros, P.; Grosse-Kunstleve, R. W.; Jiang, J. S.; Kuszewski, J.; Nilges, M.; Pannu, N. S.; Read, R. J.; Rice, L. M.; Simonson, T.; Warren, G. L. *Acta Crystallogr., Sect. D* **1998**, *54*, 905–921.
(23) Brünger, A. T. *Nature* **1992**, *355*, 472–474.
(24) Jones, T. A.; Zou, J. Y.; Cowan, S. W.; Kjeldgaard, G. J. *Acta Crystallogr., Sect. A* **1991**, *47*, 110–119.
(25) Speers, A. E.; Cravatt, B. F. *Chem. Biol.* **2004**, *11*, 535–546.
(26) Zhang, Z.-Y. *Prog. Nucleic Acid Res. Mol. Biol.* **2003**, *73*, 171–220.
(27) Zhang, Z.-Y.; Dixon, J. E. *Biochemistry* **1993**, *32*, 9340–9345.
(28) Jia, Z.; Barford, D.; Flint, A. J.; Tonks, N. K. *Science* **1995**, *268*, 1754–1758.
(29) Palmer, J. T.; Rasnick, D.; Klaus, J. L.; Bromme, D. *J. Med. Chem.* **1995**, *38*, 3193–3196.
(30) Roush, W. R.; Gwaltney, S. L., II; Cheng, J.; Scheidt, K. A.; McKerrow, J. H.; Hansell, E. *J. Am. Chem. Soc.* **1998**, *120*, 10994–10995.
(31) Frankel, B. A.; Bentley, M.; Kruger, R. G.; McCafferty, D. G. *J. Am. Chem. Soc.* **2004**, *126*, 3404–3405.

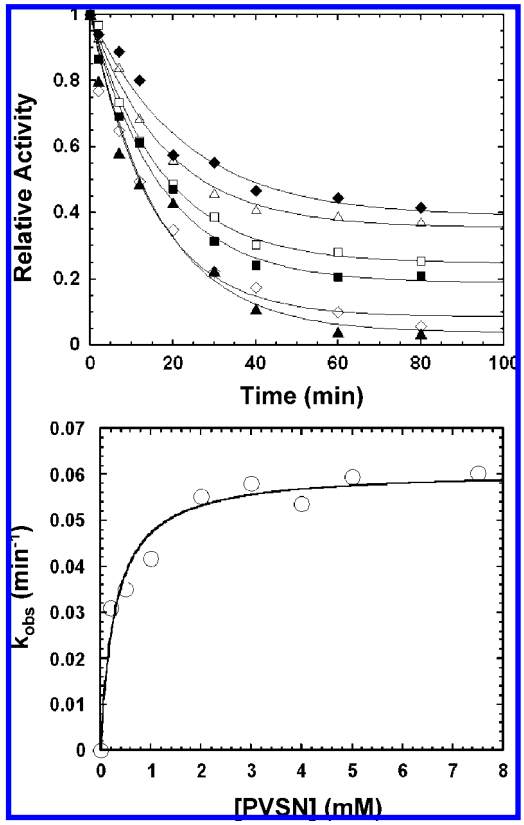

Figure 2. Kinetics of YopH inactivation by phenyl vinyl sulfonate. (A) Time and concentration dependence of YopH inactivation by phenyl vinyl sulfonate. The experimental points are represented by various symbols, and the line connecting them is the fitted line to eq 1 to yield pseudo-first-order rate constant k_{obs}. Probe concentrations were as follows: ♦, 1 mM; Δ, 2 mM; □, 3 mM; ■, 5 mM; ◇, 7.5 mM; and ▲, 10 mM. (B) Concentration dependence of the pseudo-first-order rate constant k_{obs} for phenyl vinyl sulfonate-mediated YopH inactivation. The points are experimental, and the line connecting them is the fitted line to eq 2.

inactivation rate constant k_i of 0.29 ± 0.06 mM and 0.061 ± 0.002 min^{-1}, respectively. Similar saturation kinetics was also observed for YopH inactivation by PVS (0.35 ± 0.06 mM and 0.080 ± 0.004 min^{-1} for K_I and k_i). Thus, PVSN and PVS were equally effective at inhibiting PTP activity. These results suggest that PVSN and PVS are active site-directed affinity agents whose mode of action likely involves at least two steps: binding to the PTP active site followed by covalent modification of active-site residue(s). Further evidence in support of the inactivation being directed to the active site included the observation that arsenate, a competitive PTP inhibitor, was able to protect YopH from the PVSN-mediated inactivation (Figure S1).

PVSN and PVS React with the Active-Site Cys and Form a Covalent Adduct with the PTPs. To directly demonstrate that PVSN and PVS inactivate the PTPs by covalent modification, we analyzed recombinant YopH treated with either PVSN or PVS using mass spectrometry. The molecular weight for the catalytic domain of YopH (residues 163−468) measured by an electrospray ion trap mass spectrometer was 33 514, which is in close agreement with the theoretical value (33 513). The measured molecular weights of 33 680 and 33 700 for the PVS- and PVSN-modified YopHs indicated a mass shift of 166 and 186, which correspond closely to the expected mass shift resulting from covalent attachment of PVS (mass 168.2) and PVSN (mass 184.2), respectively (Figure 3A). To identify the site of modification, YopH was incubated with or without the modifying agents, denatured in urea, reduced with DTT, alkylated with iodoacetamide, and digested with trypsin. The resulting peptides were analyzed by MALDI-TOF mass spectrometry in reflector mode. Peptide mass fingerprints were shown in Figure 3B. Peaks 1050.6, 1161.5, and 1177.2 were assigned to peptide ^{397}LRPVIHCR^{404}, in which the active-site Cys403 was covalently modified by iodoacetamide, PVS, or PVSN. To further confirm that Cys403 was the site of PVS or PVSN attachment, peptides from trypsin-digested YopH labeled with or without PVS or PVSN were analyzed by tandem mass spectrometry. Figure 3C shows the MS/MS spectra of the iodeoacetamide-, PVS-, and PVSN-modified ^{397}LRPVIHCR^{404} peptides (peaks 1050.6, 1161.5, and 1177.2 in Figure 3B). The mass differences between fragment ions b_6 and b_7 unequivocally identified Cys403 as the site of covalent modification. The results from MALDI-TOF and electrospray MS/MS experiments are consistent with the formation of a covalent adduct between YopH and PVS/PVSN involving the active-site Cys.

Structural Basis of YopH Inactivation by PVSN and PVS. To gain further insights into the mechanism of YopH inactivation by PVSN and PVS, we determined the crystal structures of YopH·PVSN and YopH·PVS complexes. Crystals of the YopH·inactivator complexes were obtained at 18 °C by the hanging-drop vapor diffusion method with 7 mg/mL of YopH that was fully modified by either PVSN or PVS (for details, see Materials and Methods). Diffraction data were then collected, and the YopH·PVSN and YopH·PVS structures were solved by molecular replacement using coordinates of YopH·*p*-nitrocatechol sulfate complex[21] as a search model and refined to 2.2 and 2.0 Å, respectively (Table 1). The final models for the YopH·PVSN and YopH·PVS complexes included YopH residues 186−468 and all atoms in PVSN and PVS. The overall structure of YopH·PVSN is comparable to the previously determined ligand-free YopH structure,[32] with root mean square derivation (rmsd) between all α-carbon positions of the two structures being 0.621 Å excluding the flexible WPD loop (residues 351−359). The major difference between these two structures is electron density in the PTP active site corresponding to PVSN, which is covalently attached to YopH via a thioether linkage between Cys403 Sγ and the terminal carbon of the vinyl group (Figure 4). The presence of electron density for this covalent adduct between PVSN and YopH was confirmed by analyzing the $2F_o - F_c$ and $F_o - F_c$ difference Fourier maps with contour levels of 1.0 and 2.5 δ, respectively (Figure 4B). Similar observations were also made with the YopH·PVS complex. The bond lengths for the thioether linkages between YopH/Cys403 and PVSN and PVS are 1.73 and 1.82 Å, respectively, which are in agreement with literature values for the C−S bond. Collectively, the structural data further support the conclusion that PVSN and PVS specifically inactivate the PTPs by modifying the active-site Cys residue.

In addition to revealing the nature of covalent linkage between YopH and PVSN/PVS, the structures also provide high-resolution views of noncovalent interactions between the active site of YopH and PVSN/PVS. As shown in Figure 5A, PVSN occupies the active-site pocket of YopH in a manner that is very similar to the way the pTyr mimetic *p*-nitrocatechol sulfate binds to YopH.[21] PVSN is inserted into an ~10 Å deep crevice that is capped by a loop from the end of strand β8 and to the first turn of helix α5, which has been termed the phosphate-

(32) Stuckey, J. A.; Schubert, H. L.; Fauman, E.; Zhang, Z.-Y.; Dixon, J. E.; Saper, M. A. *Nature* **1994**, *370*, 571–575.

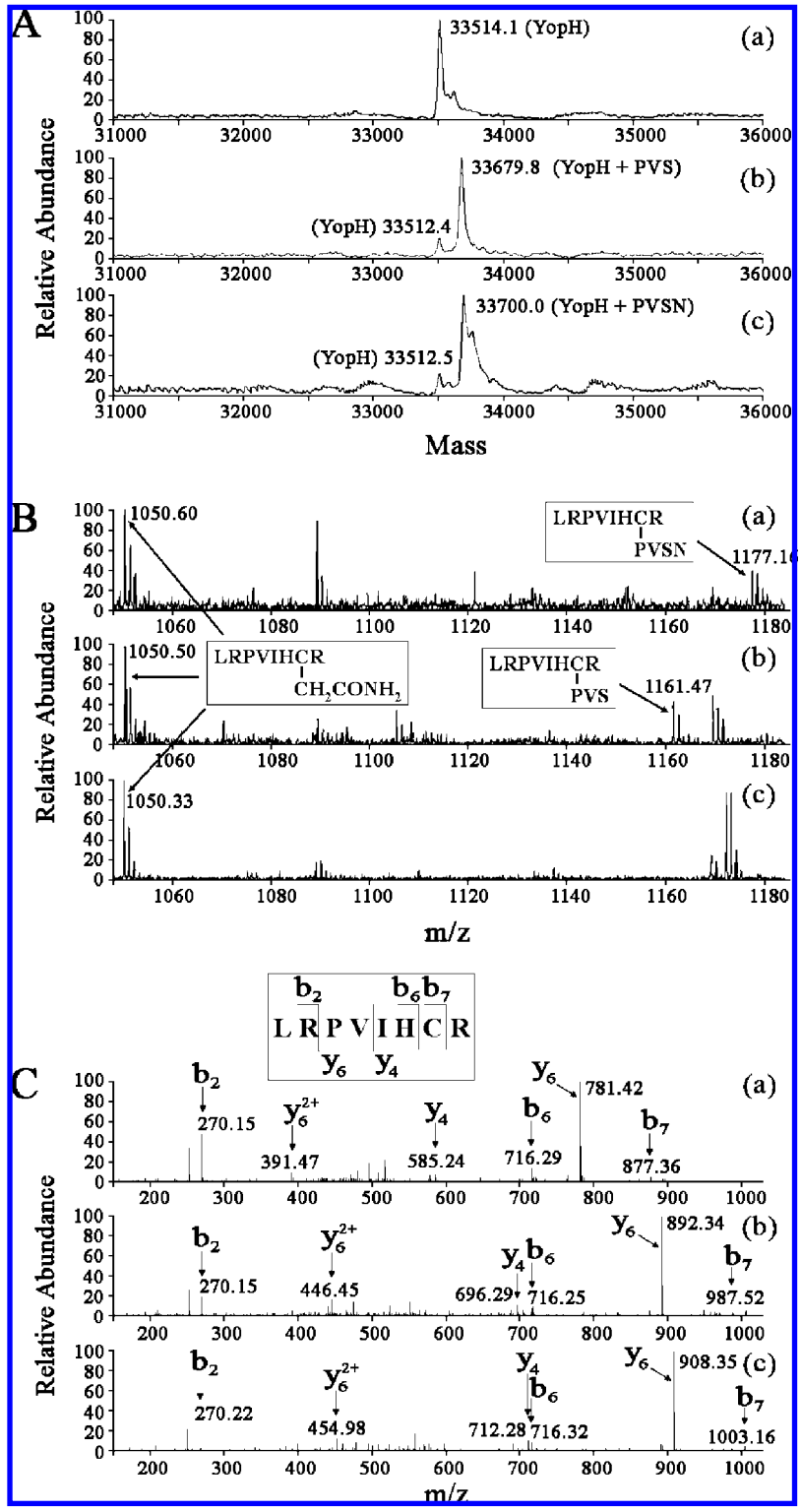

Figure 3. Mass spectrometry analyses of YopH modification by PVSN and PVS. (A) Deconvoluted ESI-ion trap mass spectra of YopH (a), YopH labeled with PVS (b) or PVSN (c). (B) MALDI-TOF spectra of trypsin-digested peptides from YopH modified by PVSN (a), PVS (b), and unmodified YopH (c). Peaks 1050.6, 1161.5, and 1177.2 were assigned to peptide ^{397}LRPVIHCR^{404}, in which the active-site Cys403 was covalently modified by iodoacetamide, PVS, or PVSN. (C) MS/MS spectra of ^{397}LRPVIHCR^{404} from the trypsin-digested YopH treated with iodoacetamide (a), PVS (b), or PVSN (c). The mass differences between fragment ions b_6 and b_7 indicate that Cys403 was the site of covalent attachment by iodoacetamide, PVS, or PVSN in YopH.

binding loop or P-loop (residues 404−409). The sulfonyl moiety is surrounded by main-chain amides of the P-loop, which donate four hydrogen bonds, the side chain of Arg409, which forms two salt bridges with the O2 atom, and a structural water molecule (Wat1) that is hydrogen-bonded to oxygen O2. Stabilized by polar interactions with the side chains of the invariant Asp356, Gln446, and Gln450, and the main-chain amide from Gln357, Wat1 is conserved and has been observed in a number of PTP inhibitor/substrate complexes.[21,28,32] At the center of the P-loop lies the catalytic Cys403, which forms a

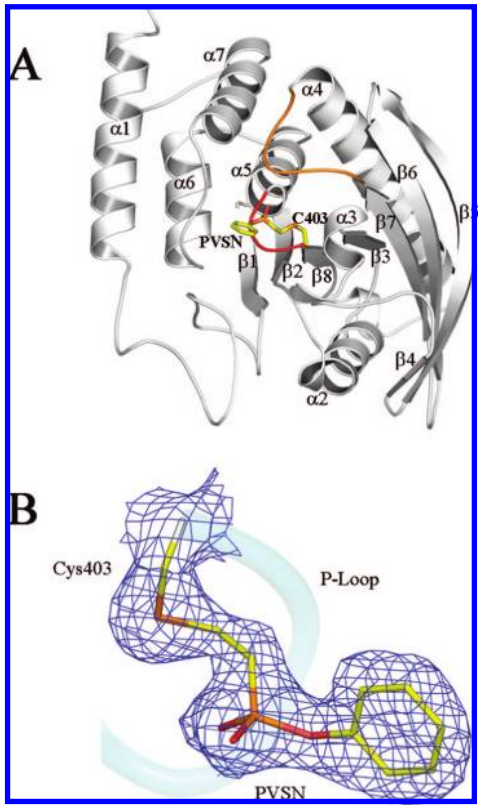

Figure 4. Crystal structure of YopH in complex with PVSN. (A) Overall structure of the YopH·PVSN complex. α-Helixes are shown in cyan, and β-sheets are shown in yellow. The P-loop and WPD-loop are highlighted in red and orange, respectively. Cys403 and PVSN are shown in stick model, and the covalent C−S bond between PVSN and Cys403 is depicted in blue. (B) Electron density map for the YopH·PVSN complex. The electron density map around PVSN and Cys403 was contoured at the 1.0 δ level in blue. Atoms were colored according to atom type (carbon in yellow, oxygen in red, sulfur in orange). P-loop was also shown with transparent cartoon in green color.

covalent bond with the vinyl group in PVSN. As observed in the YopH·*p*-nitrocatechol sulfate complex, the highly flexible WPD-loop adopts a closed conformation in the YopH·PVSN structure. In this closed conformation, the side chain of the general acid Asp356 makes two hydrogen bonds with the O2 sulfonyl oxygen and the structural water. In addition to the polar interactions, there are also van der Waals contacts between YopH and the inhibitor. The phenyl ring of PVSN makes extensive hydrophobic contacts with side chains of residues lining up the active-site cavity (i.e., pTyr binding pocket), including Phe229, Ile232, Arg404, Ala405, and Val407.

The overall structure of YopH·PVS is very similar to that of YopH·PVSN (Figure 5B), with rmsd between all α-carbon positions of the two structures at 0.365 Å. Because of the extra phenolic oxygen, the sulfonyl group in PVSN moves 0.7 Å deeper into the YopH active site and rotates 15° to the right along the phenyl ring−sulfonyl moiety axis (Figure 5C). As a consequence, the H-bonding pattern between the PVSN sulfonyl group and the YopH active site is different from that observed in the YopH·PVS structure, but the total number of hydrogen bonds in both complexes remains the same. For example, O1 in PVSN forms three hydrogen bonds with the main chain amides of Val407, Gly408, and Arg409, whereas O1 from PVS makes three hydrogen bonds with the main-chain NH groups of Gly406, Val407, and Gly408. Similarly, O2 from PVSN forms a hydrogen bond with the main-chain amide of Arg409,

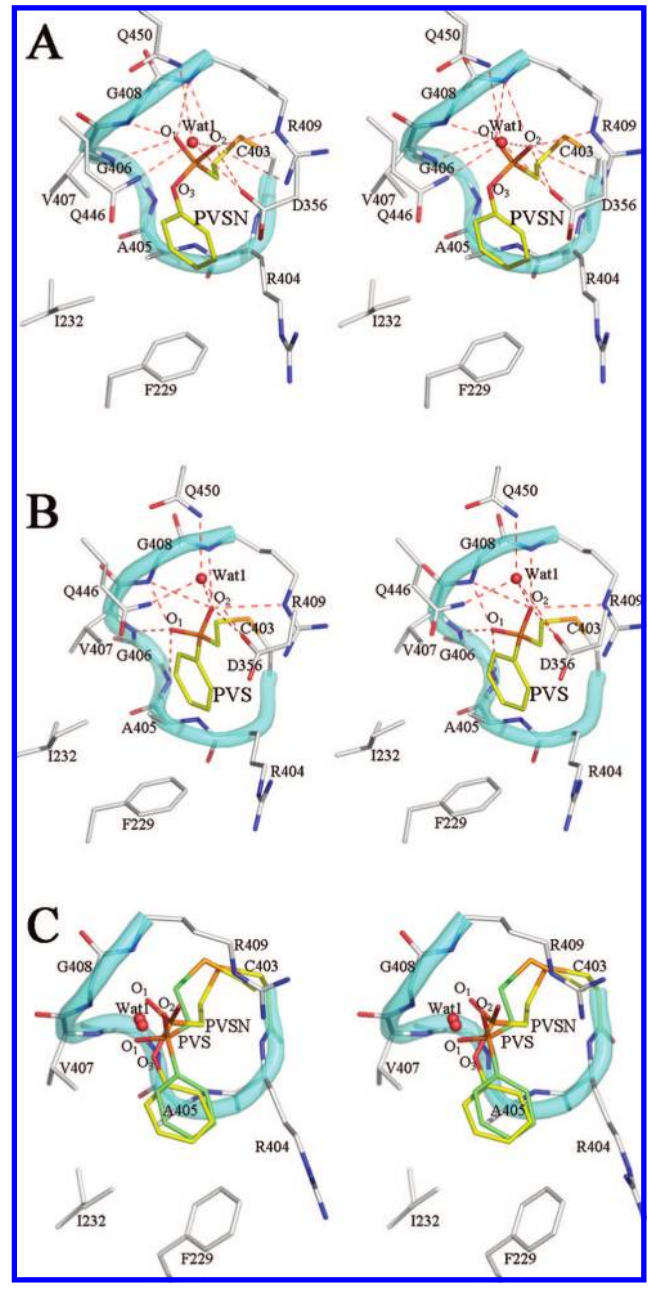

Figure 5. Detailed interactions between YopH and PVSN/PVS. (A) Stereoview of the interactions between PVSN and YopH. Hydrogen bonds and polar interactions are highlighted with dash lines in red. The covalent bond between PVSN and Cys403 is shown in orange. (B) Stereoview of the interactions between PVS and YopH. Hydrogen bonds and polar interactions are highlighted with dash lines in red. The covalent bond between PVS and Cys403 is shown in orange. (C) Superposition of the YopH·PVSN and YopH·PVS complexes. Only residues in YopH·PVSN are shown with stick model in atom color: carbon, gray; oxygen, red; sulfur, orange. The P-loop is also shown in cyan cartoon. Carbon atoms of PVSN and PVS are shown in yellow and green, respectively. Superposition was calculated with active-site residues and WPD-loop but did not include the ligands.

another one with the side chain of Asp356, and two salt bridges with the side chain of Arg409, whereas O2 from PVS forms two hydrogen bonds with the main-chain amides of Gly408 and Arg409, an additional hydrogen bond with the side chain of Asp356, and one salt bridge with the side chain of Arg409 (Figure 5A,B). Interestingly, the phenyl ring of PVS occupies almost the same position and is engaged in nearly identical van

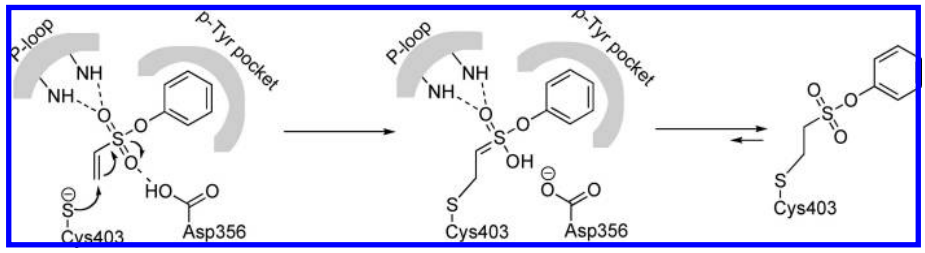

Figure 6. Mechanism of YopH inactivation by PVSN.

der Waals interactions with residues Phe229, Ile232, Arg404, Ala405, and Val407 as observed in the YopH·PVSN structure. These structural similarities between YopH·PVSN and YopH·PVS are consistent with the nearly identical kinetics of YopH inactivation exhibited by PVSN and PVS.

Mechanism and Specificity of PTP Inactivation by PVSN and PVS. It is clear from the kinetic, mass spectrometry, and X-ray crystallographic studies that PVSN and PVS can serve as efficient pTyr surrogates and specifically modify the YopH active-site Cys403. Together, our data indicate that PVSN and PVS inactivate the PTPs by electrophilic capture of the active-site Cys via 1,4-conjugate addition, forming a stable thioether adduct with the enzyme (Figure 6). A number of conserved structural features within the PTP active site contribute to specific PTP inactivation by aryl vinyl sulfonates/sulfones. The hydrophobic interactions between the phenyl moiety and the pTyr pocket are clearly important for the sulfone-mediated PTP inactivation because MVS (Figure 1) had no appreciable effect on the YopH-catalyzed *p*NPP reaction even after prolonged incubation (80 min) at 20 mM inhibitor concentration. We also noted that the first-order rate of inactivation by benzyl vinyl sulfonate (Figure 1) was 4.6-fold lower than that of PVSN. Since the intrinsic chemical reactivity of the vinyl sulfonate group is expected to be the same within the closely related benzyl and phenyl vinyl sulfonates, we attribute this decrease in rate to less favorable hydrophobic interactions between the benzyl group and the YopH active site because of the presence of an additional methylene group.

In addition to hydrophobic interactions between the phenyl ring and the pTyr binding pocket, the reactivity of PVSN and PVS toward YopH is further enhanced by specific polar interactions between the sulfonyl oxygens and main-chain amides from the P-loop and side chains of the invariant catalytic residues Asp356 and Arg409. In particular, Asp356 functions as the general acid in the PTP reaction by donating a proton to the phenolic oxygen in the leaving group.[26] In the YopH·PVS and YopH·PVSN structures, the side chain of Asp356 makes a hydrogen bond with the O2 oxygen in PVS/PVSN (Figure 5). In addition, Asp356 also contributes to the stabilization of Wat1, which is in hydrogen-bonding distance to O2. We envisaged that removal or weakening of these polar interactions would reduce the reactivity of PVSN/PVS toward YopH. We have determined the crystal structure of YopH/D356A bound to PVSN, which revealed that PVSN is covalently attached to Cys403 but Wat1 is absent in this structure (coordinates deposited in the Protein Data Bank, accession number 3BM8). Consistent with the importance of Asp356 in binding of the sulfonyl group in PVSN/PVS, an 11.7- and 9.7-fold decrease in rate was observed for the PVSN-mediated inactivation of the general acid deficient mutants YopH/D356A and YopH/D356N. Taken together, the results indicate that efficient YopH inactivation by PVSN/PVS requires both optimal hydrophobic and polar interactions between PVSN/PVS and YopH active site, which are essential to placing the terminal vinyl carbon in the immediate vicinity of Cys403 for nucleophilic attack.

Table 2. Summary of the Pseudo-First-Order Rate Constants (k_{obs}) for PTP Inactivation by 5 mM PVSN

PTPs	k_{obs} (min^{-1})
YopH	0.055 ± 0.004
PTP1B	0.047 ± 0.004
HePTP	1.66 ± 0.14
DEP1	0.036 ± 0.004
PRL1	0.163 ± 0.015
VHR	0.44 ± 0.06
LMW PTP	0.046 ± 0.008

Given the fact that the PVSN/PVS-mediated YopH inactivation takes advantage of the common structural and catalytic properties of the PTPs (e.g., pTyr binding pocket, the P-loop, Cys403, Asp356, and Arg409), it is not surprising that PVSN served as a irreversible time-dependent inactivator for all PTPs tested, including cytosolic PTP1B and HePTP, receptor-like DEP-1, the dual specificity phosphatases VHR and PRL1, and the low molecular weight PTP (Table 2). Furthermore, the ability of PVSN and PVS to engage the PTP catalytic machinery should also impart specificity of the vinyl sulfonates/sulfones toward the PTPs. Indeed, PVSN failed to inhibit the reaction catalyzed by either acid or alkaline phosphatases. PVSN was also 240−700-fold less effective in inactivating the cysteine proteases papain and cathepsin B than the mammalian PTPs HePTP and VHR (Table S1). Further elaborations of the PVSN and PVS scaffolds are expected to lead to the identification of aryl vinyl sulfonates/sulfones with increased specificity toward the PTPs.

Specificity of the PVSN-Based Probe in the Context of a Complex Proteome. To determine whether the PVSN/PVS scaffolds show specific labeling of the desired PTP in a complex mixture, we employed a novel strategy for activity-based protein profiling that utilizes the copper(I)-catalyzed azide-alkyne cycloaddition reaction ("click chemistry") to analyze the functional state of enzymes in cell lysates.[25] To this end, we prepared an azide-tagged PVSN derivative, and we appended an alkyne moiety onto biotin to facilitate click chemistry-mediated capture of the PVSN-labeled PTPs from a complex proteome (Scheme 1, and Materials and Methods). With these reagents in hand, we assessed the compatibility of the PTP labeling strategy in a well-defined system, namely *E. coli*, which has no PTPs in its proteome. The specificity of the PVSN-based probe for targeted PTP analysis was evaluated in total cell lysates from both control *E. coli* and *E. coli* expressing recombinant $(His)_6$-tagged HePTP. Total cell lysates were treated with the azide-tagged PVSN probe (20 μM) for 30 min at room temperature and pH 6.0 and exposed to 0.125 mM of the alkyne-labeled biotin, 1.25 mM TCEP, 0.127 mM TBTA,

Scheme 1. Labeling of PTPs in Complex Proteomes with the PVSN Probe by Click Chemistry

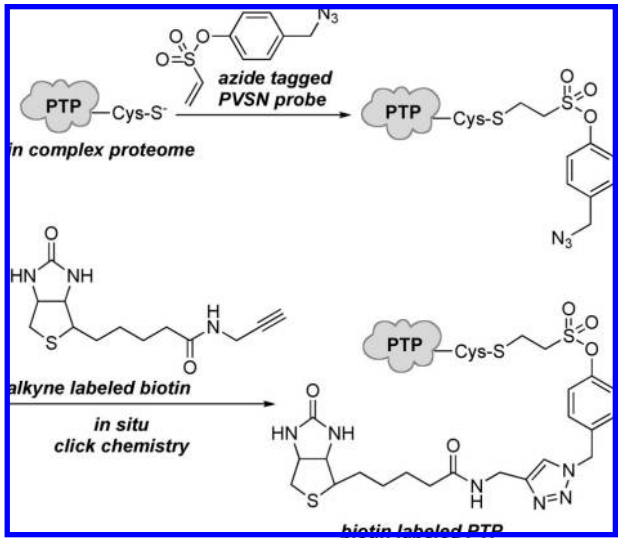

and 1.25 mM $CuSO_4$ for 1 h to conjugate the PVSN-adducted HePTP with biotin for subsequent visualization. As shown in Figure 7, Western-blot analysis of the reaction mixture with antibiotin and anti-$(His)_6$ antibodies showed robust labeling of HePTP, while little background labeling was observed for the entire non-PTP proteome under these conditions. This level of labeling specificity indicates that the PVSN/PVS scaffolds can be employed as activity-based probes to profile PTP activity in complex proteome.

Advantages of PVSN and PVS as Mechanism-Based PTP Probes. Compared to that of α-bromobenzyl phosphonate, there are several advantages associated with the aryl vinyl sulfonate/sulfone-based scaffolds. First, the kinetic parameters K_I and k_i for the PVSN (0.29 mM and 0.061 min^{-1}) and PVS (0.35 mM and 0.080 min^{-1}) mediated YopH inactivation compare very favorably to those obtained for α-bromobenzyl phosphonate (4.1 mM and 0.11 min^{-1}, respectively).[14] The 12−14-fold higher affinity exhibited by PVSN and PVS for the PTP active site indicates that they are superior pTyr surrogates. Second, α-bromobenzyl phosphonate undergoes significant solvolysis at pH greater than 7,[14] whereas PVSN and PVS are chemically inert under similar conditions, even in the presence of 1 mM glutathione (Figures S2 and S3). Third, like most pTyr mimetics, α-bromobenzyl phosphonate is negatively charged and exhibits exceedingly low membrane permeability. In contrast, PVSN and PVS are neutral pTyr mimetics and are cell permeable. Indeed, COS-7 cells treated with PVSN or PVS showed increased global tyrosine phosphorylation profiles comparable to that seen in vanadate (a commonly used potent PTP inhibitor) treated cells (Figure 8). This result supports the notion that PVSN and PVS can cross the plasma membrane and inhibit PTP activity in vivo. In contrast, MVS, an inactive analogue, and α-bromobenzyl phosphonate, which is unable to penetrate the cell membrane, had little effect on cellular tyrosine phosphorylation. Finally, unlike α-bromobenzyl phosphonate, PVSN displayed a wide range of intrinsic reactivity toward the PTPs, with k_{obs} for HePTP inactivation 30-fold greater than those for YopH, PTP1B, DEP1, and low molecular weight PTP (Table 2). This observation highlights the potential of developing isoform-selective aryl vinyl sulfonate-based PTP probes for profiling the activity of individual PTPs in signaling and in diseases.

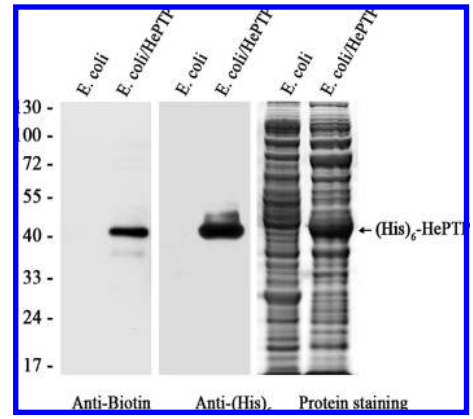

Figure 7. Labeling of HePTP in complex proteome by azide-tagged PVSN probe and alkyne-labeled biotin. Total cell lysates with or without $(His)_6$-tagged HePTP were treated with the azide-tagged PVSN probe (20 μM) for 30 min at room temperature and pH 6.0 and exposed to 0.125 mM of the alkyne-labeled biotin, 1.25 mM TCEP, 0.127 mM TBTA, and 1.25 mM $CuSO_4$ for 1 h to conjugate the PVSN-adducted HePTP with biotin. The identity of the $(His)_6$-HePTP was revealed by its reactivity to anti-$(His)_6$ antibody. PVSN labeling of HePTP was detected by antibiotin antibody.

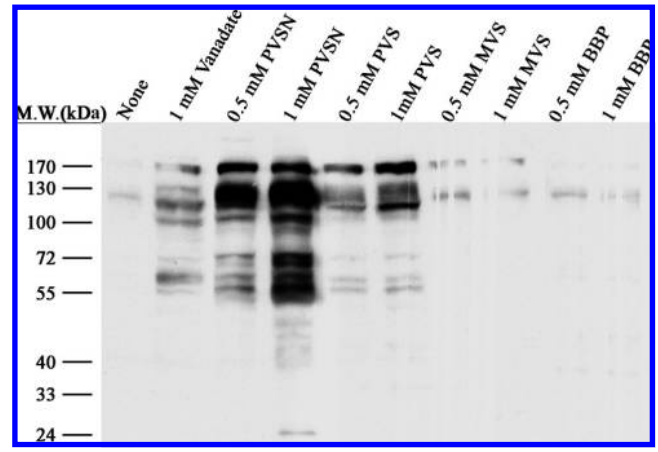

Figure 8. COS-7 cells treated with PVS or PVSN display increased tyrosine phonsphorylation. COS-7 cells were treated for 1 h with 0.5 and 1 mM PVSN, PVS, MVS, and BBP or 1 mM sodium vanadate. Cell lysate (50-μg protein) was resolved by 10% SDS-PAGE and transferred to nitrocellulose membrane. Protein tyrosine phosphorylation level was determined using anti-pTyr antibodies.

In summary, we reported kinetic and structural characterization of aryl vinyl sulfonates/sulfones as a new class of mechanism-based probes of the PTPs. We showed that PVSN and PVS inactivate a broad range of PTPs in a time- and concentration-dependent fashion. We established that this inactivation is active site-directed and irreversible. We provided evidence that PVSN and PVS form covalent adduct with the PTPs, arising from a Michael addition of the active-site Cys Sγ onto the terminal carbon of the unsaturated vinyl bond of PVSN/PVS. Our structural analysis of the YopH-inactivator complexes revealed the molecular basis for the mechanism and specificity of PVSN/PVS-mediated PTP inactivation, which lies in the ability of PVSN and PVS to take advantage of the conserved structural and catalytic properties of the PTP active site. Specific binding interactions between PVSN/PVS and the pTyr pocket position the terminal vinyl carbon in the immediate vicinity of the active site Cys for nucleophilic attack. Finally, we demonstrated that, in contrast to the α-bromobenzyl phosphonate-based

probes, PVSN and PVS are resistant to solvolysis and are cell permeable and thus hold promise for in vivo applications. Collectively, these properties bode well for the development of aryl vinyl sulfonate/sulfone-based PTP probes to interrogate PTP activity in complex proteomes.

Acknowledgment. This work was supported by National Institutes of Health Grants CA126937 and CA69202.

Supporting Information Available: Details on the effect of arsenate on the PVSN-mediated YopH inactivation, specificity of PVSN toward the PTPs and non-PTP enzymes, and stability of PVS in aqueous media and in the presence of glutathione. This material is available free of charge via the Internet at http://pubs.acs.org.

JA711125P